BULLETIN OF THE EARTHQUAKE
RESEARCH INSTITUTE
Vol. 53 (1978), pp. 649-674

33. *Surface Faulting Associated with the 1978 Izu-Oshima-kinkai Earthquake.*

By Yukimasa TSUNEISHI*, Tanio ITO** and Ken-ichi KANO**

(Received Aug. 17, 1978)

1. Introduction

A large earthquake with a magnitude of 7.0 (the 1978 Izu-Oshima-kinkai earthquake) occurred at 12^h24^m on January 14 of 1978 to the east of the Izu Peninsula. The earthquake caused severe damage to the eastern part of the Izu Peninsula, and 25 persons were killed. The damage is characterized by the collapse of mountain slopes and road cuttings (TSUNEISHI et al., 1978). The epicenter of the main shock was located at 34.8°N and 139.3°E (JAPAN METEOROLOGICAL AGENCY, 1978). The precise epicentral distribution of aftershocks was determined by TSUMURA et al. (1978). SHIMAZAKI and SOMERVILLE (1978) concluded from their seismological study that the principal energy of the earthquake was released from an east-trending right-lateral strike-slip fault 17 km long that was situated in the sea bottom between the Izu Peninsula and Izu-Oshima Island. The western extremity of the fault reached close to Inatori on the east coast of the Izu Peninsula. At Inatori a northwest-trending right-lateral strike-slip fault occurred on the ground. The occurrence of the fault on the land area was first noticed by Prof. Murai of the Earthquake Research Institute and Drs. Yoshida and Kimiya of the University of Shizuoka, independently, on the day following the main event. We carried out a precise survey of this fault. The trace of the fault mapped by us, the distribution of aftershocks and the seismologically inferred principal fault in the sea area are shown in Fig. 1.

This paper presents the study of the earthquake fault that was observed on the land area. It includes the surface trace of the fault, the distribution of measured displacements, the deformation of a railway tunnel that was truncated by the fault and the mechanical consideration on the regular arrangement of ground cracks of fault origin.

* Earthquake Research Institute.
** Geological Institute, Faculty of Science, University of Tokyo.

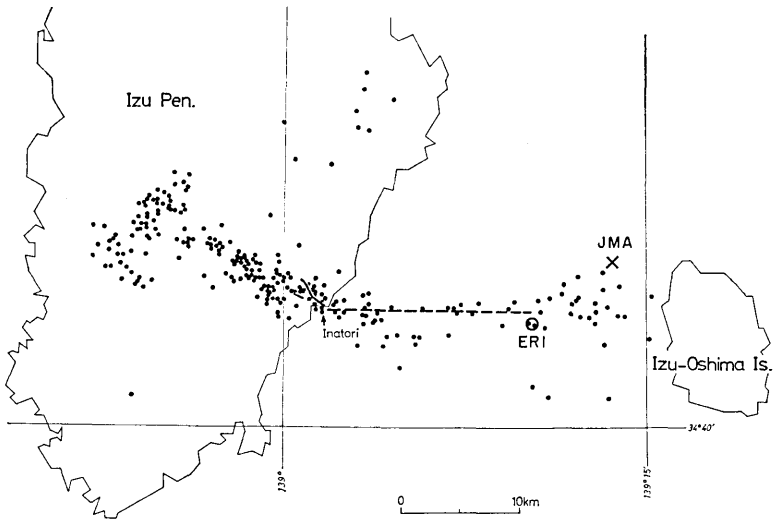

Fig. 1. Trace of the fault on the land area mapped by us (solid line), the probable principal fault seismologically inferred by SHIMAZAKI and SOMERVILLE (1978) (broken line), and the distribution of aftershocks on January 18-31 determined by TSUMURA et al. (1978). JMA and ERI designate the locations of the main shock determined by JAPAN METEOROLOGICAL AGENCY (1978) and TSUMURA et al. (1978), respectively.

The Izu Peninsula is geologically founded on submarine volcanic sediments of the Miocene Yugashima and Shirahama Groups, and is covered by many Quaternary volcanoes. The surface geology of the faulted area is composed of the Pleistocene andesitic lava and volcanic mudflow deposits. Izu-Oshima Island is an active basaltic volcano.

2. Surface Trace of the Fault

As shown in Fig. 2, the fault observed on the land area is traced northwestward for about 3 km from the coast at Inatori. More precisely, it runs N 55°W for 1.5 km from the coast to Iriya and N 30°W from there on, but it turns N 55°W near its northwestern termination. Another strand lies at Neginota.

On the ground surface, the fault is manifested by a group of regularly arranged ground cracks and displaced man-made structures. Individual cracks are generally a few meters long and essentially tension fractures. The regular en-échelon arrangement of these cracks constitutes a fissure zone of 100-700 meters length. In Fig. 2 fissure zones

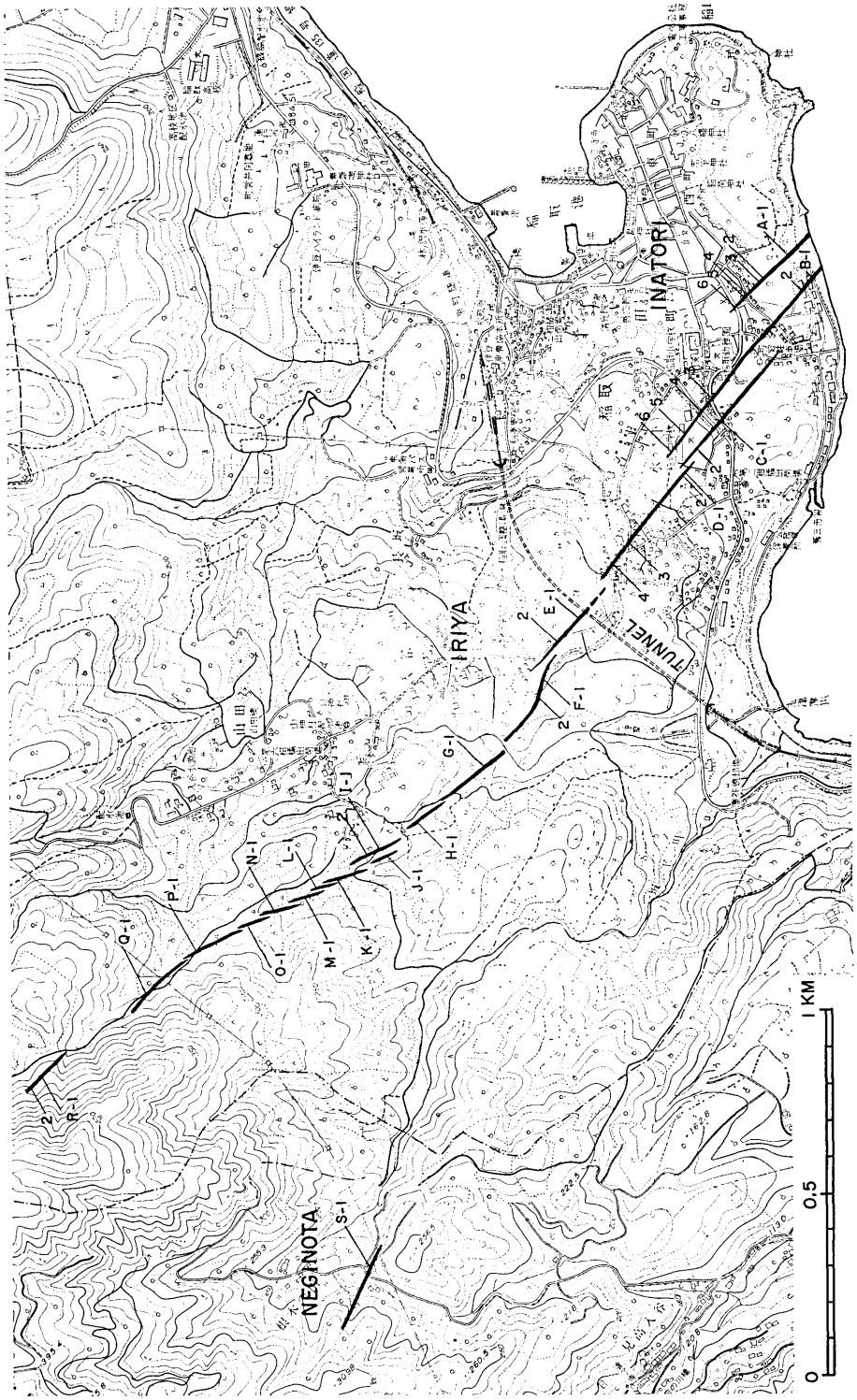

Fig. 2. En-échelon fissure zones at Inatori. Letters and figures denote the locations of displacement measurements.

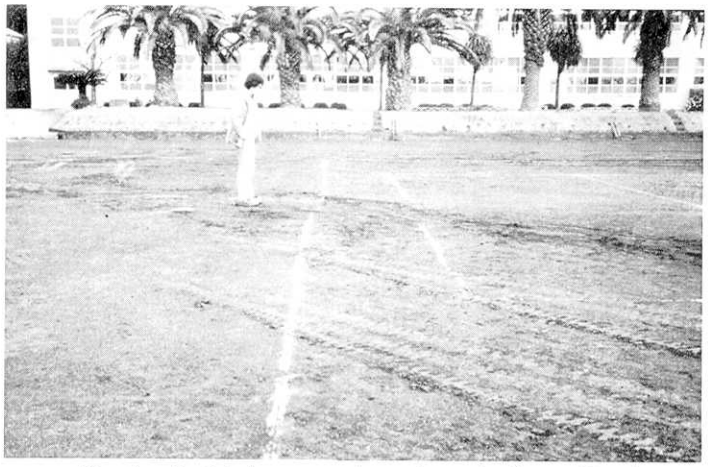

Fig. 3. En-échelon ground cracks and offset white lines on the playground of Inatori Junior High School (Loc. C-2).

Fig. 4. En-échelon ground cracks on the surface of a country lane (Loc. G-1).

Fig. 5. En-échelon ground cracks on the surface of an orange field (100m north-northwest of Loc. G-1).

Fig. 6. Pressure ridge formed between adjacent en-échelon ground cracks (Loc. F-2).

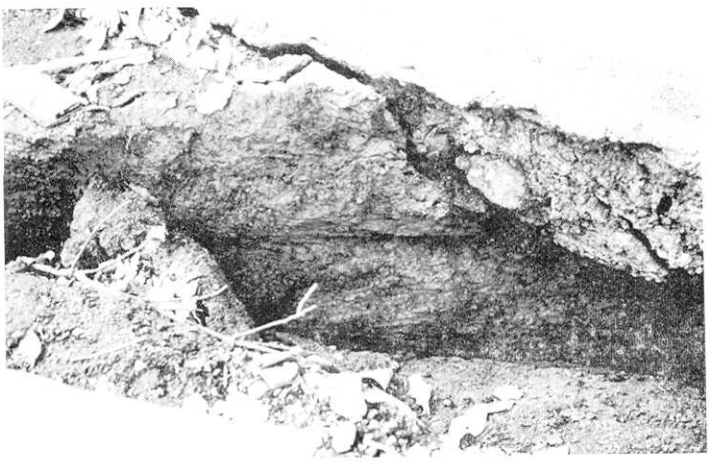

Fig. 7. Slickensided surface on the side wall of a ground crack (Loc. F-2).

Fig. 8. Displacement of a small cliff in the backyard of a house (Loc. S-1).

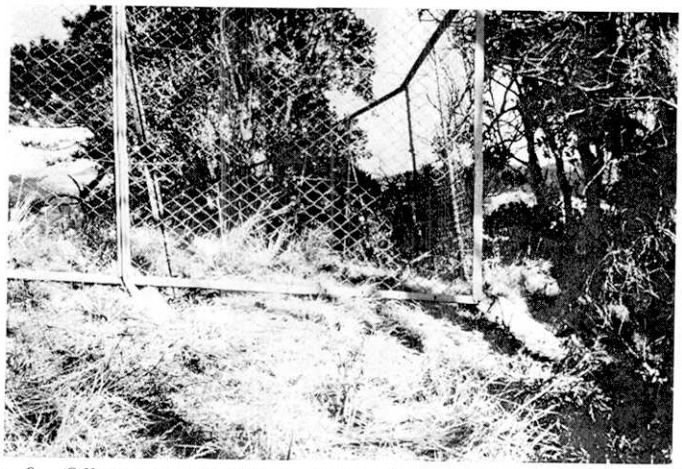

Fig. 9. Offset and stretched fence of a tennis court (Loc. A-1).

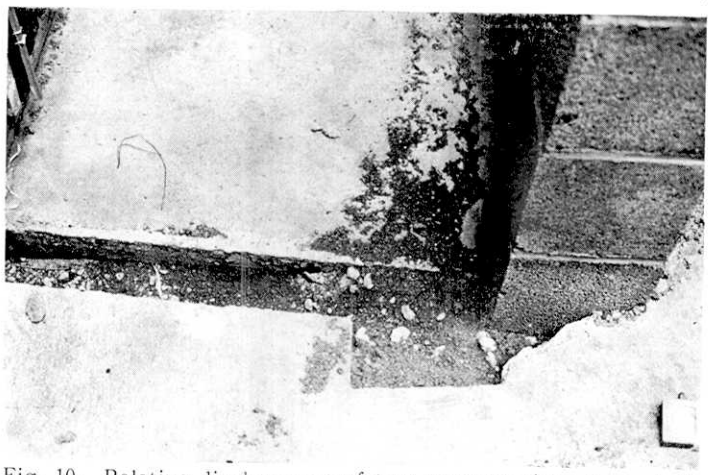

Fig. 10. Relative displacement of two concrete slabs (Loc. A-3).

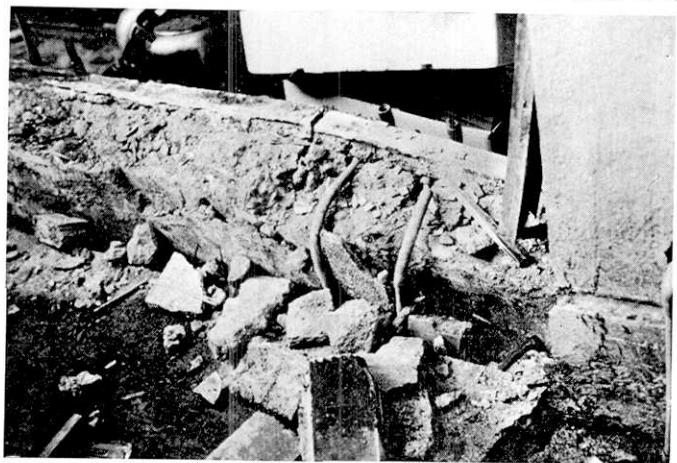

Fig. 11. Disrupted and offset wall of a building of reinforced concrete (Loc. B-2).

are indicated by solid lines, and designated alphabetically. They are distributed en-échelon within a narrow belt of 30–200 m width, below which we inferred a burried fault. Thus, the surface trace of faulting is double échelon in pattern, inasmuch as the zones of en-échelon cracks are themselves distributed in an en-échelon pattern.

The trend of individual fissure zones is oblique to the inferred fault about 10° in a clockwise sense, whereas the trend of individual cracks is oblique to the corresponding fissure zone about 20°–30° in a clockwise sense. The manner of en-échelon arrangement, as well as the displacement of man-made structures, indicates that the fault is a right-lateral strike-slip fault.

In the following, typical examples of fissured ground surfaces and deformed man-made structures are presented. Fig. 3 shows en-échelon ground cracks and curved white lines on the playground of Inatori Junior High School (Loc. C-2 of Fig. 2). Fig. 4 shows en-échelon ground

Fig. 12.

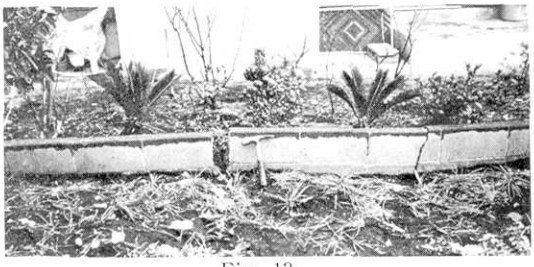

Fig. 13.

Fig. 14.

Fig. 12. Offset pavements of the Higashi-Izu Highway. Two cracks in a near view occurred due to displacement of fissure zone-C (Loc. C-1).

Fig. 13. Displaced and stretched partition of a flower bed (Loc. D-1).

Fig. 14. Thrusting up of a concrete slab onto the pavement of a road (Loc. D-3).

cracks on the surface of a country lane (Loc. G-1). Fig. 5 shows another example of en-échelon ground cracks on the surface of an orange field (100 m north-northwest of Loc. G-1). Fig. 6 shows a pressure ridge formed between adjacent en-échelon ground cracks (Loc. F-2). Pressure ridges are evidence of local compressional effects within the fissure zone. At the same locality, a slickensided surface was observed on the side wall of a ground crack (Fig. 7). At Neginota a small cliff in the back-yard of a house was fissured and offset right-laterally, as shown in Fig. 8 (Loc. S-1).

Where man-made structures were deformed by the fault movement, various features of disruption occur depending on the kind of the structures and the angle of intersection between the fault and the structures. Fig. 9 shows a displaced and stretched fence surrounding a tennis court (Loc. A-1). The fence is oblique to the fissure zone in a counterclockwise sense. Fig. 10 shows the relative displacement of two concrete slabs (Loc. A-3). The joint between the two concrete slabs is oblique to the fissure zone in a clockwise sense. Fig. 11 shows a complexly disrupted and right-laterally displaced wall of a building of reinforced concrete (Loc. B-2). The wall stands nearly perpendicular to the fissure zone. Fig. 12 shows the displaced portion of a paved road (Loc. C-1). Another displacement of the road by fissure zone-B (Loc. B-3) is seen in a distant view. Fig. 13 shows a displaced and stretched partition of a flower bed (Loc. D-1). The partition is oblique to the fissure zone in a counter-clockwise sense. Fig. 14 shows thrusting up of a concrete slab onto the

Fig. 15. Roadside concrete slab rotated and buckled in a chevron shape and the central main slab rotated in a clockwise sense (Loc. E-2).

Fig. 16. Displaced stone wall in an orange field (30 m northwest of Loc. P-1).

pavement of a road (Loc. D-3). The direction of thrusting is oblique to the fissure zone in a clockwise sense. Fig. 15 shows features of a deformed road pavement (Loc. E-2). Fissure zone-E traversed the road from the upper left corner to the lower right corner of the photo. The road was shortened in a longitudinal direction and was extended in a lateral direction. The roadside concrete slab buckled in a chevron shape and the central main slab rotated in a clockwise sense. Fig. 16 shows a displaced stone wall in an orange field (30 m northwest of Loc. P-1).

A vinyl hothouse was obliquely traversed and distorted by fissure zone-I at Loc. I-2. Fig. 17(a) shows a sketch map of the vinyl hothouse of which three corners are lettered a, b and c. The fissure zone traversed the western corner-b of the hothouse and displaced the adjacent walls. Fig. 18 shows the displaced wall a-b on the southwestern side of the hothouse. The fault movement not only offset the walls, but lengthened the wall a-b and shortened the wall b-c. The pillars in the walls are aligned at an interval of 2 meters. The bases of the pillars are fixed on the ground and the tops are attached to the crossbeams. Because the tops of pillars are restrained by the crossbeam, the pillars lean over from the vertical position, as shown in Fig. 19. Conversely, we are able to determine the relative displacement of the ground by setting a temporary vertical line from the top of the pillar and measuring the distance between the foot of the pillar and the vertical line. Fig. 17(b) shows the result of measurement. The direction

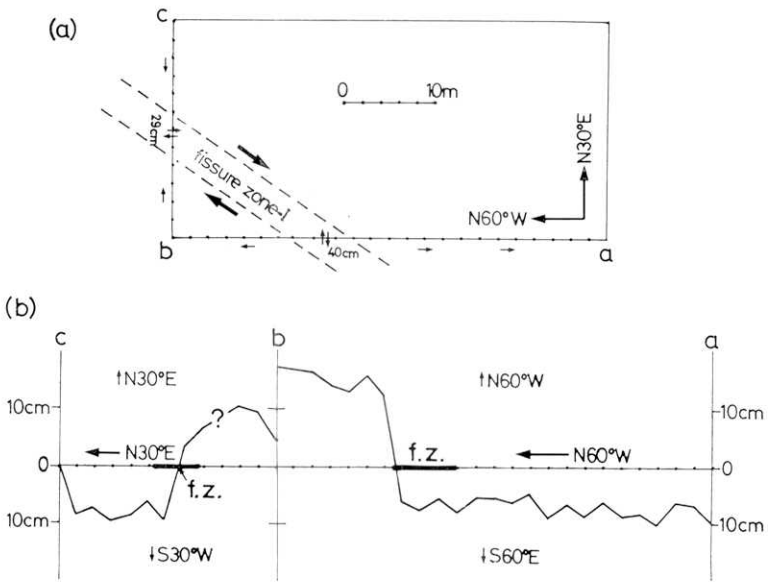

Fig. 17. (a) : Sketch map of a deformed vinyl hothouse (Loc. I-2).
(b) : Displacement of pillars due to faulting.

Fig. 18. Displaced wall a-b of the hothouse shown in Fig. 17.

Fig. 19. Close view of one of the hothouse's pillars leaning away from a vertical position (Loc. I-2).

of the displacement is clearly different on opposite sides of the fissure zone.

3. Displacement of the Fault

Because the present fault is manifested on the ground surface by a group of doubly arranged en-échelon cracks, we cannot directly measure the amount of displacements along the fault. Instead, we can observe displacements of fissure zones and estimate the displacement of the fault from them. In cases where previously adjoined, but now separated points are identified across a ruptured man-made structure, we are able to measure the three-dimensional displacement vector (Fig. 20-a). Examples are given at Loc. A-3 (Fig. 10) and Loc. C-1 (Fig. 12). At Loc. E-2 (Fig. 15) we were able to measure the amounts of shortening and lengthening along perpendicular directions, respectively. In such a case we can compose them as a vector and get the resultant displacement. The above-mentioned three examples are included in Table 1.

The direction of displacements, represented in Table 1, is about 10° oblique to the direction of the related fissure zones in a counterclockwise sense. That is to say, the fissure zones have an opening component in addition to a right-lateral strike-slip component. Thus, the displacements become parallel to the fault, because the trend of the fault is about 10° counterclockwise oblique to the trend of fissure zones except for fissure zone-F which is parallel to the fault on its central portion. Now we accept the following three assumptions: (1) the displacement along the fault is pure strike-slip, (2) it is virtually equal to the displacement along fissure zones in its direction and value, and (3) the direction of the fault is truly 10° oblique to the direction of fissure zones except for fissure zone-F. With these three assumptions, the data on the displacement of the fault greatly increase, because we can then utilize many data that are otherwise defective to determine three-dimensional displacements of the fault.

Table 1. Fault displacements obtained as a unique solution.

Loc. No.	Horizontal Displacement	Trend of Fissure Zone
A—3	N 55°W, 21 cm	N 40°W
C—1	N 60°W, 18 cm	N 50°W
E—2	N 58°W, 26 cm	N 50°W

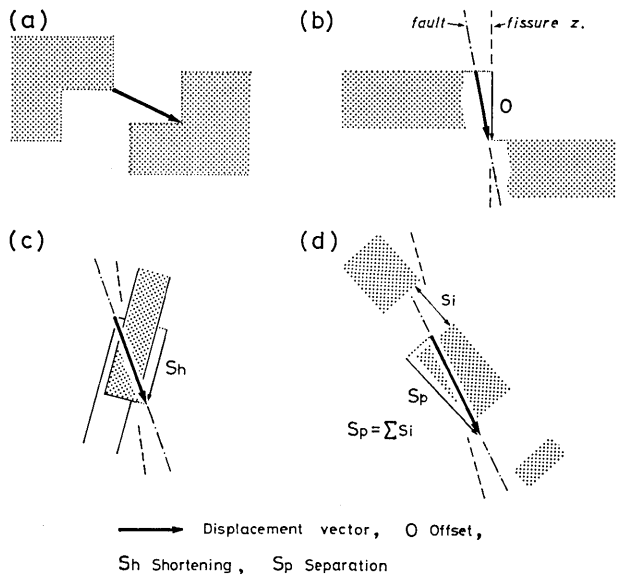

Fig. 20. Four types of fracturing of man-made structures and their relation with displacement vector. See the text for details.

Generally, deformational features of linear man-made structures due to faulting differ according to the angle of intersection between the structure and the fault. As shown in Fig. 20-b, when a fissure zone intersects a linear structure roughly at right angles, we can easily measure the amount of offset of the displaced segments. Since the amount of offset changes with the angle of intersection and with the opening component across the fissure zone, we cannot estimate the displacement of a fissure zone or a fault only by the amount of offset. However, based on the above-mentioned three assumptions we can determine the amount of displacement of the fault from the direction of offset, its amount and the direction of the fissure zone.

When a fissure zone intersects a linear man-made structure at acute angles, the structure is lengthened or shortened, as shown in Fig. 20-c, d. In such an instance, we can determine the fault displacement from the direction of lengthening or shortening, its amount and the direction of the fissure zone on the three assumptions.

The estimated values of the fault displacement are summarized in Table 2. As for the type of estimation, refer to Fig. 20. The calculation on fissure zone-F was done on the exceptional assumption that the fissure

Table 2. Estimated values of the fault displacement.
Alphabetical signs in the column of Calculating Method correspond to the same signs in Fig. 20.

Fissure Zone		Loc. No.	Calculating Method	Displacement	
Name	Trend			strike-slip (cm)	dip-slip (cm)
A	N 40°W	1	d	89	
		2	b	26	
		3	a	21	6
		4	b	11	
		5	d	14	
		6	d	12	
B	N 50°W	1	d	32	10
		2	b	31	16
		3	d	10	
		4	d	11	
		5	d	10	
		6	b	6	
C	N 50°W	1	a	18	
		2	b	23	
D	N 50°W	1	d	17	
		2	b	21	
		3	c	34	
		4	d	16	
E	N 50°W	1	d	19	
		2	c + d	29	
F	N 50°W	1	c + d	51	10
	N 72°W	2	a	52	7
G	N 30°W	1	b	51	10
H*	N 30°W	1	b	52	20
I	N 25°W	1	d	56	
		2	b	56**	
J*	N 20°W	1	b	10	
K*	N 15°W	1	b	36	
L*	N 15°W	1	b	102	
M*	N 15°W	1	b	128	
N*	N 10°W	1	b	70	20
O*	N 20°W	1	b	90	
P*	N 25°W	1	b	76	10
Q*	N 50°W	1	c	62	
R	N 50°W	1	b	55	
		2	c	60	
S	N 65°W	1	c + d	8	

* : Maximum amount of strike-slip displacement along the fissure zone.
** : Mean of two values.

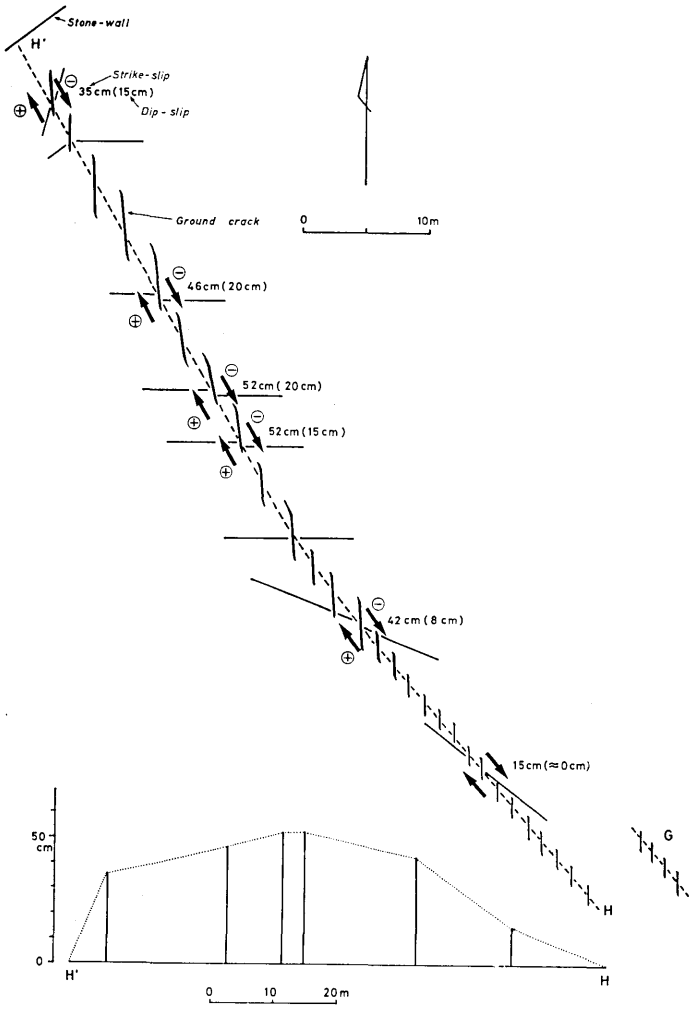

Fig. 21. En-échelon ground cracks on fissure zone-H and the distribution of displacement. ⊕ and ⊖ denote up-thrown and down-thrown sides, respectively.

zone is parallel to the fault. As for the vertical component of the displacement, the northeastern block has consistently moved down with a maximum amount of 20 centimeters.

Fissure zones-H and K were precisely mapped, as shown in Figs. 21 and 22, in order to examine the distribution of displacement along the fissure zones. The amount of displacement is distributed rather evenly along the fissure zones and diminishes at the terminations.

The distribution of displacement along the fault is shown in Fig. 23. In places where adjacent fissure zones overlap, the sum of the amounts

of displacement along them is indicated as a solid square in Fig. 23. The amount of displacement attains a maximum of 128 centimeters on fissure zone-M and diminishes from there, but it increases again toward the coast. Fig. 23 also shows the amount of displacement of a railway tunnel. The amount of displacement observed in the tunnel is consistent with the values measured on the ground surface.

4. Deformation of the Inatori Tunnel due to Faulting

It is very rare that a tunnel is deformed due to faulting. In Japan, one case has been recorded in which the Tanna Tunnel under construction was displaced by the Tanna Fault in the 1930 Kita-Izu earthquake. The present fault associated with the 1978 Izu-Oshima-kinkai earthquake traversed the

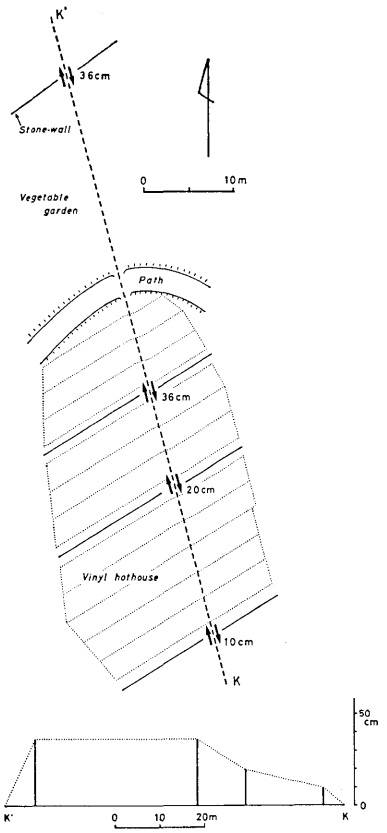

Fig. 22. Sketch map of fissure zone-K and the distribution of displacement.

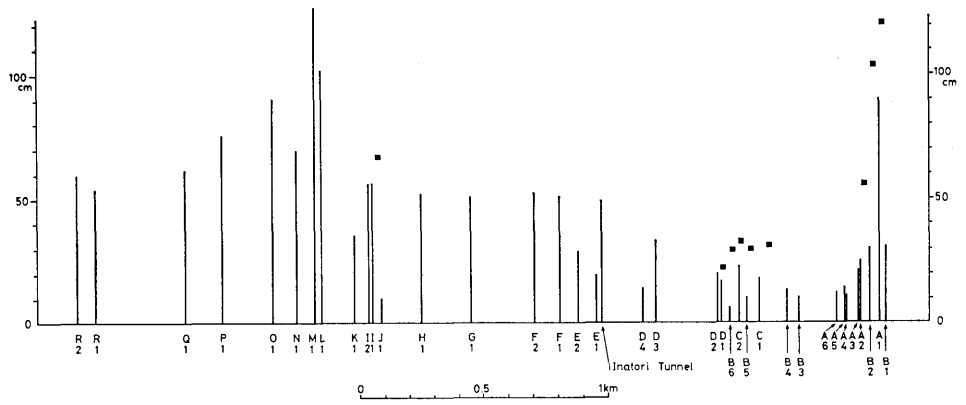

Fig. 23. Distribution of displacement along the fault. See the test for the mark of solid squares.

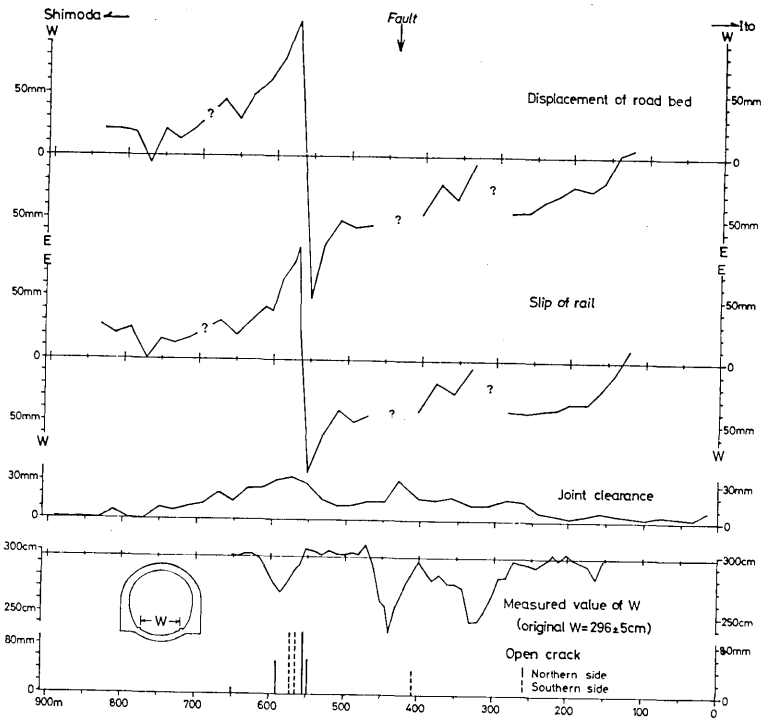

Fig. 24. Tectonic features of deformation of the Inatori Tunnel. The left and right sides of the figure correspond to the SW and NE entrances of the tunnel, respectively. See the text for details.

Inatori Tunnel of the Izu Kyuko Line and severely deformed it. The engineering aspect of the damage to the tunnel has been reported by ONODA et al. (1978), and so we describe tectonic features of the deformation in the following.

The Inatori Tunnel is a single track railway tunnel of 906 meters in length. Its location is shown in Fig. 2. Fig. 24 shows the results surveyed by us. The axis of abscissa expresses the distance from the northeastern entrance of the tunnel.

The concrete lining of the tunnel was fractured in many places in a complicated manner (Figs. 25 and 26). Among those fractures we picked up tension cracks that occurred on the side walls of the tunnel and measured their openings. Open cracking is concentrated in the section 540–590 m, as shown in Fig. 24. The most conspicuous open crack observed on the side wall of the tunnel is 9 cm wide (Fig. 27).

Deformation of the cross section of the tunnel was also surveyed by measuring the distance W between the edges near the bed of the tunnel (see the sketch inserted in Fig. 24). The measured values of

Fig. 25. Exfoliation of the concrete lining of the tunnel.

Fig. 26. Squeezing up of ballast due to lateral pushing of the side wall of the tunnel.

distance W are plotted in Fig. 24. The distance W is smaller near three points 330 m, 440 m and 580 m than its original value of 296 ± 5 cm. The maximum decrease reaches 62 cm at the point 440 m. These phenomena resulted from the destruction of the inverted arch of the tunnel due to lateral compression. The geology around the tunnel consists of volcanic mud flow deposits that have been altered into clay by hydrothermal action. The complicated deformation of the tunnel is probably ascribed to the particular mechanical property of faulted bedrocks around the tunnel.

Fig. 27. Open crack on the side wall of the tunnel.

Rails can be utilized as a measure in surveying the deformation of the tunnel. However, since rails are jointed with a definite clearance, it is necessary to estimate the change of the joint clearance that occurred with faulting. In fact, the joint clearance was enlarged abnormally, as shown in Fig. 28. Fig. 24 shows the result of measurement of the joint clearance. The joint clearance has become larger near the point 430 m and section 550–600 m. This fact means that rails were stretched at the joints in the vicinity of these portions. Because readjustment of joint clearances has not been done since the construction of the tunnel in 1961, the distribution of joint clearances just prior to faulting is unknown. Thus in calculating the change of joint clearances we used the value of 6 mm clearance with which rails were originally laid.

A railway track is composed of a roadbed, ballast, rail-ties, tie-plates and rails. Although the rails are tightened onto rail-ties by dog-spikes, a strong force is able to make a rail slip on a rail-tie in a longitudinal

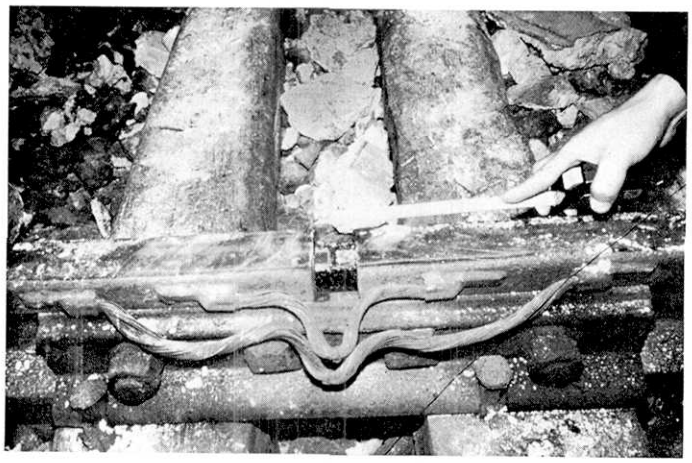

Fig. 28. Abnormally enlarged joint clearance.

Fig. 29. Slipping of a rail on the tie-plate as revealed by the scratch of the dog-spike on the flange of the rail.

direction. In the Inatori Tunnel, such a slipping of rails was observed extensively, as shown in Fig. 29. As the surface of a rail is coated with oil and dust, we can easily measure the amount of slipping and its direction from the scratch of the dog-spike on the rail flange. Occasionally where tightening between a rail and a rail-tie is strong or the slip is large, even the rail-tie has moved, shoving ballast ahead. In such cases, we can roughly estimate the displacement of the rail-tie by measuring the gap that formed between the rail-tie and the pile of ballast at the rear of the rail-tie.

The displacement of a rail relative to the roadbed, which was estimated in the above-mentioned way, is shown in Fig. 24. The amount of displacement is given as the sum of the value obtained from the scratch of dog-spikes and the value obtained from the dislocation of rail-ties. Moreover, the average value of measurements on the two parallel rails is shown. The direction of slip of rails is also indicated in Fig. 24.

The amount of slip of rails, shown in Fig. 24, increases toward the point 560 m, and the direction of slip abruptly changes at that point. However, the amount of slip of the rails does not denote the displacement of the tunnel, because rails are elongated at their joints. Hence the cumulative increments of joint clearance over the original value of 6 mm should be added to the slip of the rails. The result is given in the uppermost figure of Fig. 24. The amount of elongation of the tunnel reaches 22 cm at the point 560 m. The value is nearly equal to the sum of the openings (20 cm) of the side wall of the tunnel.

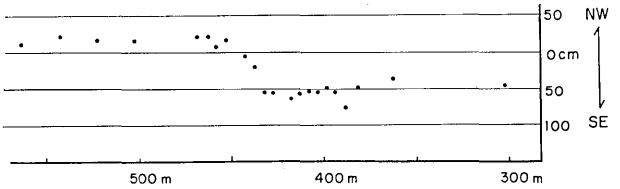

Fig. 30. Displacement of the tunnel center at the rail level. (after ONODA et al., 1978)

The precise survey of the deformed tunnel was done by the Izukyu Corporation (ONODA et al., 1978). Fig. 30 shows that the center of the tunnel at the rail level was displaced right-laterally by 50–70 cm within the zone 20 m of the point 440 m. Right-lateral deformation of the tunnel should result in lengthening the tunnel. Many exfoliations of the concrete lining as shown in Fig. 25 occurred near the point 440 m. However, the position of the actual extensional deformation of the tunnel determined by the relative slip of rails lies 120 m southwest (point 560 m) of the position of the lateral shifting of the tunnel detected by the precise surveying. This discrepancy is explained as follows.

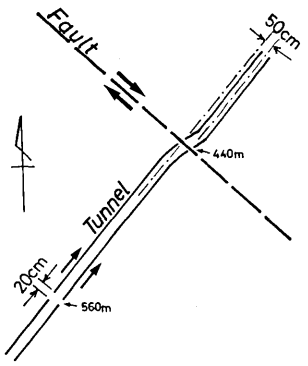

Fig. 31. Schematic diagram of the deformation of the tunnel.

Fig. 31 shows the deformation of the tunnel diagrammatically. The fault is considered to have traversed the tunnel and deformed it at the point 440 m where lateral displacement of the tunnel was detected by the precise survey, because the location roughly coincides with the trace of the fault observed on the ground surface that lies 90 m above the tunnel. It is probable that the concrete lining of the tunnel between the points 440 m and 560 m slipped to the northeast through the bedrock of hydrothermally altered mud flow deposits, and was eventually torn at the point 560 m. Horizontal striations were observed on the surface of the bedrock behind the concrete lining when the fractured slab of lining was removed for the repair of the tunnel (personal communication of Mr. Takagi). This fact supports the above-mentioned inference.

Precisely speaking, the observed trace of the fault is located on the ground surface above the point 470 m. On the other hand, the fault traversed the tunnel at the point 440 m underground. At that point the

tunnel lies 90 m below the ground surface. Hence the dip angle of the fault is estimated to be 72° toward the northeast.

Another conspicuous deformation of the tunnel occurred near the southwestern entrance of the tunnel. Between the points 858 m and 898 m the railway track was made to meander, as shown in Fig. 32. The joint clearances in this portion became null. Therefore, the deformation of the track is considered to have been brought about by buckling in a longitudinal direction. The amount of shortening was estimated to be 16 cm by Prof. Tamura (personal communication). The arch and side walls of the tunnel were split along the spring level. The arch has moved 5–10 cm relative to the side walls toward the southwestern entrance of the tunnel. A side-ditch on the roadbed of the tunnel was also buckled. These phenomena indicate that the roadbed of the tunnel was shortened in a longitudinal direction within this portion. But on the ground surface we could not discover a distinct fault trace such as associated with the shortening of the tunnel.

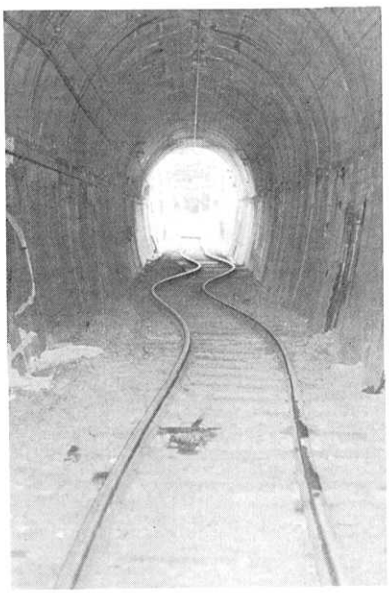

Fig. 32. Meandering of the railway track between the points 858 m and 898 m. (taken by T. Takagi)

5. Double Echelon Arrangement

The surface manifestation of the fault associated with the 1978 Izu-Oshima-kinkai earthquake is characterized by the double échelon arrangement of ground cracks; that is to say, individual ground cracks of the tension fracture type are arranged en-échelon and making fissure zones, and the fissure zones themselves are also arranged en-échelon. A double échelon arrangement of ground cracks due to faulting has been reported in the Matsushiro earthquake fault associated with the activity of the swarm earthquakes of 1966 in Matsushiro (TSUNEISHI and NAKAMURA, 1970). However, in the present earthquake the double échelon arrangement was developed in a far more typical shape. Development of the double échelon arrangement is theoretically examined in the following

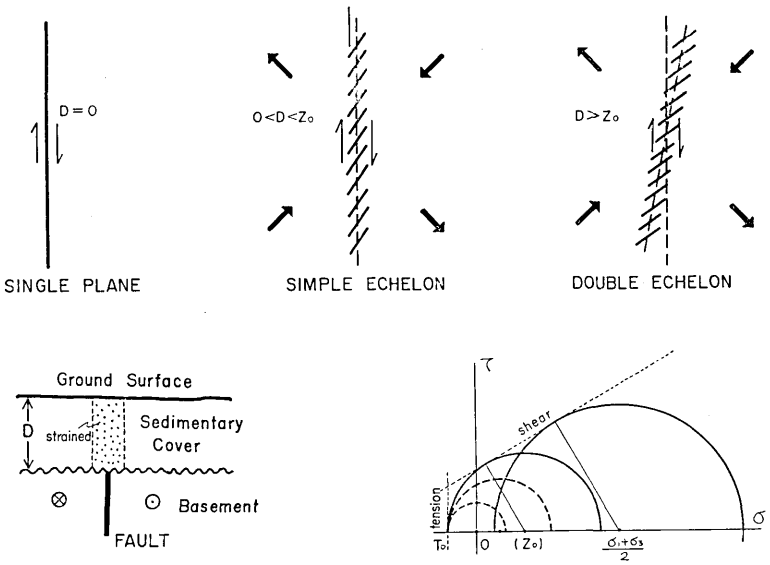

Fig. 33. Schematic diagram explaining the formation of double échelon arrangement of ground cracks.

paragraphs.

In general there are three types of surface manifestation of faulting: a single plane, a simple échelon arrangement and a double échelon arrangement. The distinction is presumed to occur according to the thickness of the sediments covering the faulted bedrock. We assume that the bedrock has a single fault plane and that the covering sediments were accumulated after the preceding faulting occurred, as shown in Fig. 33. In case that no sediments cover the bedrock, the surface trace of faulting is expressed by faulting of the bedrock itself and results in a single fault plane. In case that the bedrock is covered by sediments and that the displacement along the fault is small, a simple or double échelon arrangement of ground cracks develops on the ground surface, because the tension strength is generally smaller than the shear strength.

Mohr's circle representation is used in the following mechanical treatment of stress state. Before faulting begins, one of the principal stresses is vertical in the sedimentary cover, whereas the other two principal stresses lie in a horizontal plane and are equal to each other. When strike-slip faulting occurs in the bedrock, the overlying sedimentary cover is deformed and strained. The maximum compressive principal stress σ_1 and the minimum one σ_3 develop in a horizontal plane and are disposed in 45° directions to the direction of the fault. Now we assume

that $(\sigma_1+\sigma_3)/2$ is constant in the course of deformation and proportional to the depth of the point within the sedimentary cover.

As the strain increases in the sedimentary cover, the radius of Mohr's circle increases but the center of the circle remains fixed. When the circle reaches the fracture line, the sedimentary cover is fractured. There are two fracture lines, shear and tension. When $(\sigma_1+\sigma_3)/2$ is small, tension fracture occurs. On the other hand, when $(\sigma_1+\sigma_3)/2$ is large, shear fracture occurs.

As shown in Fig. 33, a critical value of $(\sigma_1+\sigma_3)/2$ corresponding to the depth Z_0 determines which of the two types of fracture occurs. When thickness D of the sedimentary cover is smaller than the critical depth Z_0, a simple échelon arrangement of tension fractures results. When the thickness D of the sedimentary cover is larger than the critical depth Z_0, a group of shear fractures develop in the deeper portion of the sedimentary cover. The direction of the shear fractures is about 10° oblique to the direction of the fault in the bedrock because of internal friction. Thus the direction of fissure zones is determined.

The shear fractures will be arranged en-échelon in the deeper portion of the sedimentary cover. Shearing along the shear fractures deforms and strains the upper portion of the sedimentary cover and develops a group of en-échelon tension fractures along the individual shear fractures. Thus the double échelon arrangement of the ground cracks results.

6. Concluding Remarks

The fault associated with the 1978 Izu-Oshima-kinkai earthquake has a length of about 3 km in a northwest direction on the land area. It is a right-lateral strike-slip fault with a maximum displacement of 128 cm. As for the vertical displacement, the northeastern block has moved down with a maximum amount of 20 cm. On the other hand, the principal fault of the earthquake is presumed to have occurred in an east-west direction in the sea area (SHIMAZAKI and SOMERVILLE, 1978). The two faults are acutely bent at their junction, as shown in Fig. 1. Therefore, the part of the fault on the land area is possibly a derivative fault of the principal fault in the sea area. In addition the trace of the fault on the land area is composed of three bent segments. This suggests that preexisting fault blocks have been unlocked along their boundary faults by the movement of the principal fault. We consider that the earthquake fault on the land area was derived from the principal fault in the sea area.

Acknowledgements

We are very grateful to Prof. T. Kimura of the Geological Institute, University of Tokyo, for a critical reading of the manuscript. We are also indebted to Prof. J. Tamura of the Institute of Industrial Science, University of Tokyo, Mr. T. Kusuyama, the chief of the Construction Section, Izukyu Corporation, and Mr. T. Takagi of the Environmental Assessment Center Co. Ltd. for providing information on the deformed Inatori Tunnel.

References

JAPAN METEOROLOGICAL AGENCY, 1978, The Seismological Bulletin of the Japan Meteorological Agency for January 1978.

ONODA, K., T. KUSUYAMA and K. YOSHIKAWA, 1978, Damage to railway tunnels due to the Izu-Oshima-kinkai earthquake, *Tunnel and Underground*, **9**, 375-380. (in Japanese)

SHIMAZAKI, K. and P. SOMERVILLE, 1978, Summary of the static and dynamic parameters of the Izu-Oshima-kinkai earthquake of January 14, 1978, *Bull. Earthq. Res. Inst.*, **53**, 613-628.

TSUMURA, K., I. KARAKAMA, I. OGINO and M. TAKAHASHI, 1978, Seismic activities before and after the Izu-Oshima-kinkai earthquake of 1978, *Bull. Earthq. Res. Inst.*, **53**, 675-706. (in Japanese with English abstract)

TSUNEISHI, Y. and K. NAKAMURA, 1970, Faulting associated with the Matsushiro swarm earthquakes, *Bull. Earthq. Res. Inst.*, **48**, 29-51.

TSUNEISHI, Y., T. ITO and K. KANO, 1978, Slope collapses along the main roads of the Izu Peninsula caused by the 1978 Izu-Oshima-kinkai earthquake, *Bull. Earthq. Res. Inst.*, **53**, 1069-1084. (in Japanese with English abstract)

---

33. 1978年伊豆大島近海地震によって陸上に出現した断層

地震研究所　恒石　幸正
東京大学理学部地質学教室　伊藤　谷生，狩野　謙一

1978年1月14日に生じた伊豆大島近海地震（M＝7.0）によって，伊豆半島東部の東伊豆町稲取付近と河津町根木の田に地震断層が出現した（第2図）．稲取付近に出現した断層は稲取海岸から北西に3km ほど追跡できる．より詳しく見ると，稲取海岸から入谷までの 1.5 km では N55°W，入谷から北 1.5 km では N30°W の走向を有し，断層の北端部では再び N55°W となる．

地表では，この断層は規則的に配列した亀裂群をつくり，人工構造物を変位させている．個々の亀裂は本質的にはテンション・フラクチャーで，一般に数 m の長さを持っている．亀裂は規則的なエシェロン状の配列を示し，100-700 m の長さの亀裂帯を作っている．この亀裂帯がさらにエシェロン状の配列を作り，この下に地下での断層が推定される．このように，地表での断層の表現は見事な二重雁行のパターンを有している．

個々の亀裂帯は地下に推定される断層の走向に対し，時計まわりに約10°斜交している．また，個々の亀裂は，亀裂帯の走向から 20°～30° 程度時計まわりに斜交している．このようなエシェロン状の配列形態と人工構造物の変位は，この断層が右横すべり断層であることを示している．

亀裂，亀裂帯の例として，稲取中学校校庭(第3図)や，みかん畑に生じたもの(第5図)等が示された．人工構造物は，断層の走向との交叉角度により，さまざまな形の変形を示す．この変形例として，断層の走向と反時計まわりに斜交するテニスコートの柵(第9図)や花壇の変形(第13図)，時計まわりに斜交するコンクリートスラブの変形(第14図)などが示された．また，断層の走向とほぼ平行する道路面の変形(第15図)や，直交するみかん畑の石垣の変形(第16図)などが示された．さらに断層上に，断層と斜交して建てられたビニールハウスの側面の変形例(第17図)が示された．

断層の変位量は亀裂帯の変位量から推定される．その詳しい方法は本文に述べられている．亀裂帯の走向と直交する人工構造物の変位はほぼそのまま亀裂帯の右横すべり変位量として見積ることができる．斜交する場合や平行する場合は，構造物に生じた開口量や，短縮量を計測する．これらの計測値をもとに，本文に述べられた一定の仮定をおいて地下での断層の右横すべり変位量を計算することができる．このようにして計算された断層の変位量分布が第23図に示されている．2つの亀裂帯が，オーバーラップして分布している場合には，両者で得られた変位量を積算した値が第23図に■印で示されている．最大変位量は断層の中央部からやや北側の部分で 128cm に達し，その両側に向かって減少していくが，南東部では再び稲取海岸にむかって増大している．垂直変位量は最大 20cm で北東側が下降している．

次に断層が横切った伊豆急行線稲取トンネル（全長 906 m）の変形が記載された．伊東側坑口から 540～590 m のトンネル側壁には開口割れ目が発達していた．トンネルの幅員は 330 m，440 m，580 m の地点で著しく短縮し，440 m ではその短縮量が 62 cm にも達した．さらにレールを基準として路盤の変位量を推定するために，レールの遊間や，レールと枕木との間の水平移動量と方向，さらに，枕木のずれを計測した．レールは 560 m 地点で突然その移動方向を逆にしている．これから計算される 560 m 地点でのトンネルの伸び量は 22 cm であり，同地点でのトンネル側壁の開口量 20 cm と調和している．以上のトンネル内での計測結果は第24図に示されている．

トンネル中心線の変位を精密測量によって求めた結果(第30図)によると，トンネルは440 m 地点で 50～70 cm の右ずれ変位を示している．この地点でトンネルの変状が著しいことと，この地点の地表付近に断層の通過が認められることを合わせて考えると，トンネル内では断層は 440 m 地点を通過したものと判断される．そうすると，560 m 地点に現われた開口状の変形は，440 m 地点での屈曲に要したトンネルの軸長の変化が何らかの機構によって 120 m はなれた地点へ移された結果と考えなければならない．トンネル掘削時の工事記録によると地山の地質は温泉余土化した泥流堆積物と推定される．したがって，第31図に模式的に示すように，トンネルのライニングは線路と共に地山の中を 560 m 地点から 440 m 地点まで引きずられたのではなかろうか．トンネルの復旧工事の際，外されたライニングの後側に露出した地山の面には水平な擦痕が見られたという．

トンネル内で推定された断層の位置と地表での確認点とを結ぶと，断層は北東方向へ72°傾斜していることになる．トンネル内で認められる変位量と地表での変位量とはほぼ等しい．

なお，下田側坑口に近い 858 m から 898 m の区間ではレールの屈曲がみられた(第32図)．ここでは約 16 cm 路盤が長軸方向に短縮したと推定されるが，この短縮をひきおこしたかも知れない断層は地表では発見できなかった．

つぎに，横すべり断層による亀裂の二重雁行配列の成因が考察された(第33図)．基盤の中にはすでに一枚の断層面が形成されていて，これが再活動するが，基盤をおおう被覆層にはまだ断層面ができていないとする．被覆層の厚さがゼロ，すなわち基盤が地表に露出している場合には，地表での断層は単一面として表われる．被覆層が薄い場合には，断層はテンションクラックの単純な雁行配列として現われる．被覆層が厚い場合には，被覆層の下部では雁行する剪断破壊面が形成され，亀裂帯の位置と方向が定まる．さらに，個々の剪断破壊面について，被覆層の上部では，テンションクラックの雁行配列が生じ，二重雁行配列が完成すると考えられる．

単純雁行か二重雁行かは被覆層の厚さによってきまることが，応力のモール円表示(第33図)によって示される．被覆層中の水平面内に直交する主応力 σ_1 と σ_3 を考える．変形開始前には，$\sigma_1=\sigma_3$ とする．基盤の断層運動によって，被覆層は歪み，$\sigma_1-\sigma_3$ は増大するが $(\sigma_1+\sigma_3)/2$ の値は不変であると考えてよい．つまり，モール円の中心は変形を通じて動かないとする．モール円が剪断の破壊線と引張の破壊線とのいずれに早く接するかによって，破壊の種類がきまるのであるが，それは出発点の円の中心の位置によって決定される．円の中心の位置は初期応力によってきまるので，深

さの関数であると考えてよい．被覆層の力学的物性によって，破壊線の位置はきまる．そのうえで，二重雁行配列が発生するに必要な被覆層の厚さが決定される．

SHIMAZAKI and SOMERVILLE (1978) は今回の地震のエネルギーのほとんどは，伊豆半島と大島との間の海域を東西にのびる長さ17kmの断層から解放されたことを地震学的に結論している．第2図にみられるように，この主断層に対して，陸上で観察された地震断層は鋭く折れ曲っている．また，陸上に出現した断層は屈曲する3個のセグメントより成る．これらのことより，陸上で観察された断層は，既存の地塊構造を区画する境界断層が主断層の運動によって誘発され，再活動した派生断層であると考えられる．

付記： 今回の地震断層についての調査報告のなかには，稲取北方の浅間山南西斜面上部に左ずれの「浅間山断層」が出現したとするものが見受けられる．しかし，その実体は表層地辷りによる亀裂群であって，断層の地表的表現とは認められない．